

# Comparison of electrical explosions of Cu and Al wires in water and glycerol

D. Yanuka, A. Rososhek, and Ya. E. Krasik  
 Physics Department, Technion, Haifa 32000, Israel

(Received 31 March 2017; accepted 21 April 2017; published online 5 May 2017)

The results of experiments on single Cu and Al wire electrical explosions with a current density of  $\sim 10^8$  A/cm<sup>2</sup> in water and glycerol on ns- and  $\mu$ s-timescales are presented. Framing and streak images of the exploding wires and generated shock waves were used for the analysis of the possible contribution of Al and glycerol combustion to the shock wave velocity and pressure behind its front. It was shown that on nanosecond and microsecond timescales of wire explosions, one obtains Al and glycerol combustion. However, Al combustion does not contribute to the velocity of the generated shock wave because of a relatively slow rate of energy density deposition into the water flow. Nevertheless, electrical explosion of Al and Cu wires in glycerol showed a significant increase in the generated shock wave velocity and consequently in the pressure behind its front as a result of glycerol's higher density and combustion. *Published by AIP Publishing.*  
[\[http://dx.doi.org/10.1063/1.4983055\]](http://dx.doi.org/10.1063/1.4983055)

## I. INTRODUCTION

Underwater electrical explosion of a single wire, characterized by extremely large energy density deposition, can be used for studies of equations of state (EOS) and parameters of a warm dense plasma with a coupling coefficient  $\Gamma > 1$ .<sup>1–3</sup> Also, underwater electrical explosion of either a cylindrical or spherical wire array is accompanied by the generation of a shock wave (SW) whose convergence results in an extreme state of water in the vicinity of the implosion axis or origin.<sup>3</sup>

In earlier experimental research<sup>4–7</sup> on underwater electrical explosions of Cu and Al single wires and wire arrays, carried out on nanosecond (ns) and microsecond ( $\mu$ s) timescales, it was supposed that Al wires' explosion can result in additional energy transferred to the generated SW and water flow due to Al combustion. However, no detailed research on this subject has been carried out yet. Also, one can consider electric explosion of wires in another medium whose combustion may lead to such an additional energy transfer.

In this paper, we present the results of experimental research of single Cu and Al wires' underwater electrical explosions in water and glycerol. The data obtained are compared with the results of hydrodynamic simulations coupled with EOS of water, Cu, and Al, and estimates are made on the energy which can be realized due to Al combustion. We also show that the use of glycerol as the medium in which wire explosions are carried out allows one to obtain significantly larger velocities of the generated SW and consequently higher values of pressure behind the SW front.

## II. EXPERIMENTAL SETUP

The research was carried out using ns- and  $\mu$ s-timescale pulse generators. The ns timescale generator is based on a Marx generator, which charges a water forming line.<sup>4</sup> This generator produces at its output a high voltage (HV) pulse of 120 kV, 50 kA, and  $\sim 80$  ns pulse duration at a 1.5  $\Omega$  matched resistive load at a charging voltage of 30 kV of the Marx generator. The  $\mu$ s-timescale generator includes 4 low-inductance

high-voltage (HV) capacitors of 0.22  $\mu$ F each, connected in parallel, and a triggered spark gas switch. The discharge of these capacitors (charging voltage up to 30 kV) on a single wire results in a current pulse with an amplitude of up to 25 kA and a rise time of 1.2  $\mu$ s. The experimental setup is shown in Fig. 1.

The powerful pulse delivered either by the ns- or  $\mu$ s-time-scale generators is applied to a wire stretched between HV and ground electrodes placed in a stainless steel chamber filled with tap water. In the case of wire explosion in glycerol, single-use 50  $\times$  45  $\times$  40 mm perplex boxes with the wire stretched between electrodes placed at the sides were used. These boxes were filled with glycerol and placed between the HV and ground electrodes in the same chamber filled with tap water.

The discharge current  $I$  through the wire was measured using a low-inductance coaxial current viewing resistor (0.125  $\Omega$ ) placed at the side of the ground electrode, and the voltage drop  $\phi$  across the exploding wire was measured using a Tektronix HV voltage divider connected to the HV electrode. The shadow images of the exploding wires and generated SW were obtained using a fast framing intensified camera (4QuikE) operating with a frame duration of 2–5 ns at different time delays with respect to the beginning of the discharge current. Also, a streak camera (OptoScope SC-10) operating with different streak timescales was used to obtain shadow and light-emission images of the expanding channel of the exploding wires and propagation of the generated SWs. For the back-lighting of the exploding wire and SW, a 155 mW diode-pumped, 532 nm CW laser (MGL-III-532) was used.

## III. EXPERIMENTAL RESULTS

### A. Nanosecond timescale underwater electrical explosions of Cu and Al wires

To obtain a critically damped discharge allowing the fastest energy density deposition rate into the wire, preliminary estimates of the wire's cross-section and length based

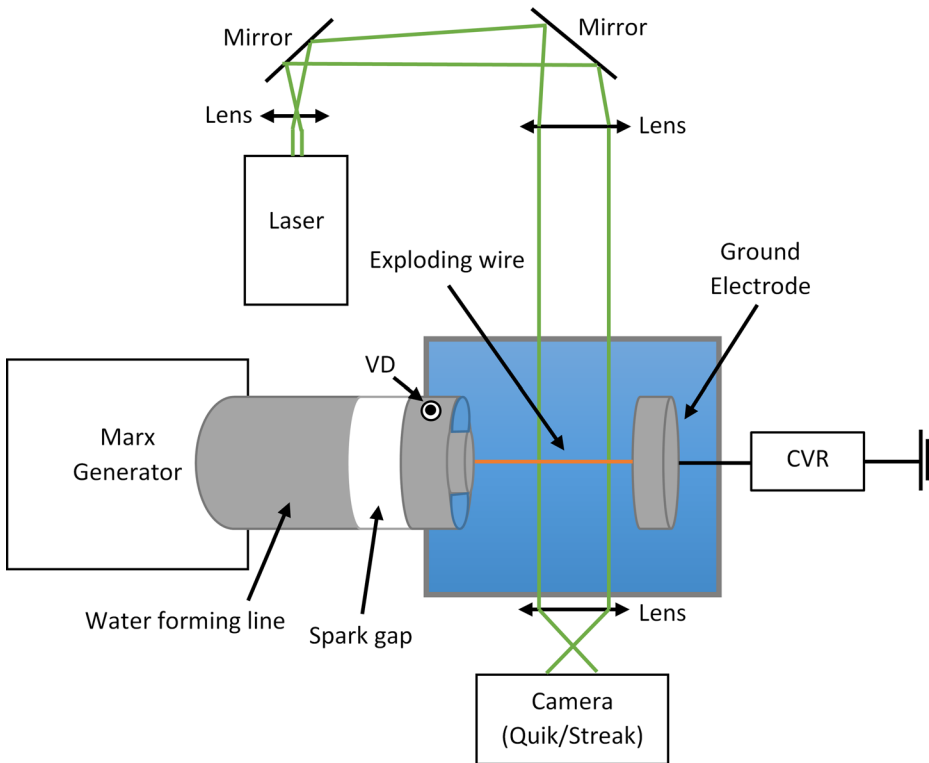


FIG. 1. Experimental setup. CVR is the current view resistor, and VD is the output from the high voltage electrode connected to the Tektronix high-voltage divider.

on the specific current action<sup>8</sup> and the energy conservation law were made together with a few preliminary explosions of wires in water. It was found that a critically damped discharge is obtained with 100  $\mu\text{m}$  and 127  $\mu\text{m}$  diameters for Cu and Al wires, respectively, having lengths of 45 mm. The obtained specific current action values  $h = \int_0^{t_{\text{exp}}} j^2(t) dt$ , where  $j(t)$  is the current density in the wire and  $t_{\text{exp}}$  is the time of explosion, are  $\sim 2.54 \times 10^9 \text{ A}^2 \text{ s/cm}^4$  and  $\sim 1.3 \times 10^9 \text{ A}^2 \text{ s/cm}^4$  for Cu and Al wires, respectively. These specific current action values are slightly different from the corresponding values of  $3 \times 10^9 \text{ A}^2 \text{ s/cm}^4$  for Cu and  $9 \times 10^8 \text{ A}^2 \text{ s/cm}^4$  for Al presented in Refs. 8 and 9. This discrepancy can be related to the rather sophisticated dependence of the specific current action on parameters of the discharge current density. On the one hand, the increase in the energy deposition rate and current density results in the increase in the value of  $h$ ,<sup>9,10</sup> but on the other hand, the value of  $h$  decreases in the case of the skin effect resulting in non-linear magnetic field diffusion.<sup>11</sup> The latter can be realized in the present experiment due to an extremely large self-magnetic field ( $>40 \text{ T}$ ) of the discharge current. Let us note that the ratio  $h_{\text{Cu}}/h_{\text{Al}} \approx 2.2$  presented in Ref. 8 is close to the ratio  $h_{\text{Cu}}/h_{\text{Al}} \approx 2.5$  obtained in the current experiment.

Typical waveforms of the discharge current and resistive voltage,  $\phi_r = \phi_w - L_w dl/dt$ , where  $L_w$  is the wire inductance which was assumed to be almost constant during the wire explosion and  $\phi_w$  is the total measured voltage for the cases of Cu and Al wires' electrical explosion in water, are shown in Figs. 2(a) and 2(b). Also, in Figs. 2(a) and 2(b), the temporal evolution of the wires' resistance which increases with a rate of  $\sim 10^8 \text{ } \Omega/\text{s}$ , reaching a maximal value of  $\sim 5 \text{ } \Omega$ , is shown. The average current density estimated at the time of explosion, i.e., at the beginning of the decrease in the discharge current, is  $\sim 3.5 \times 10^7 \text{ A/cm}^2$  and  $\sim 3.1 \times 10^7 \text{ A/cm}^2$

for the cases of Al and Cu wire explosions, respectively. The time dependent power and energy deposited into the Cu and Al wires are shown in Figs. 2(c) and 2(d). One can see that the total energy deposited into the Cu and Al wires is almost the same  $\sim 90 \text{ J}$ , but the energy densities are different, namely, in the case of the Al wire, one obtains  $\sim 52 \text{ kJ/g}$  ( $\sim 14 \text{ eV/atom}$ ) and in the case of the Cu wire, it was  $\sim 25.4 \text{ kJ/g}$  ( $\sim 17 \text{ eV/atom}$ ). Here, let us note that one requires  $\sim 22.3 \text{ J}$  and  $\sim 15.6 \text{ J}$  for complete vaporization of the Cu and Al wires, respectively, which are significantly smaller than the deposited energy.

Shadow frame images (see Figs. 3(a), 3(b), 4(a), and 4(b)) showed the axial uniformity of the discharge channels and generated SWs for Cu and Al wires' electrical explosions in water and glycerol. One can see that neither strata formation typical for thermal instabilities nor hydrodynamic instabilities was observed. These data confirmed that a background environment like water or glycerol prevents fast wire radial expansion keeping large density of the wire, thus decreasing significantly increments in these instabilities, typical for wire explosion in vacuum or gas.<sup>12</sup>

The shadow streak images (see Figs. 3(c) and 3(d)) showed that the SW's velocities and wire's radial expansions were almost the same (difference  $<1.3\%$ ) for Cu and Al wires in the same medium. However, when comparing these velocities between water and glycerol, we obtained faster SW velocity and wire radial expansion in the latter (see Figs. 3 and 4). The radial trajectories of the expanding Cu wires and generated SWs for explosions in water and glycerol are shown in Fig. 5.

One can see that during the time  $t \leq 300 \text{ ns}$  with respect to the beginning of the discharge current, the SW radial expansion velocity in glycerol coincides with its velocity in water. However, later in time, one obtains faster propagation velocity of the SW in glycerol. The latter can be explained

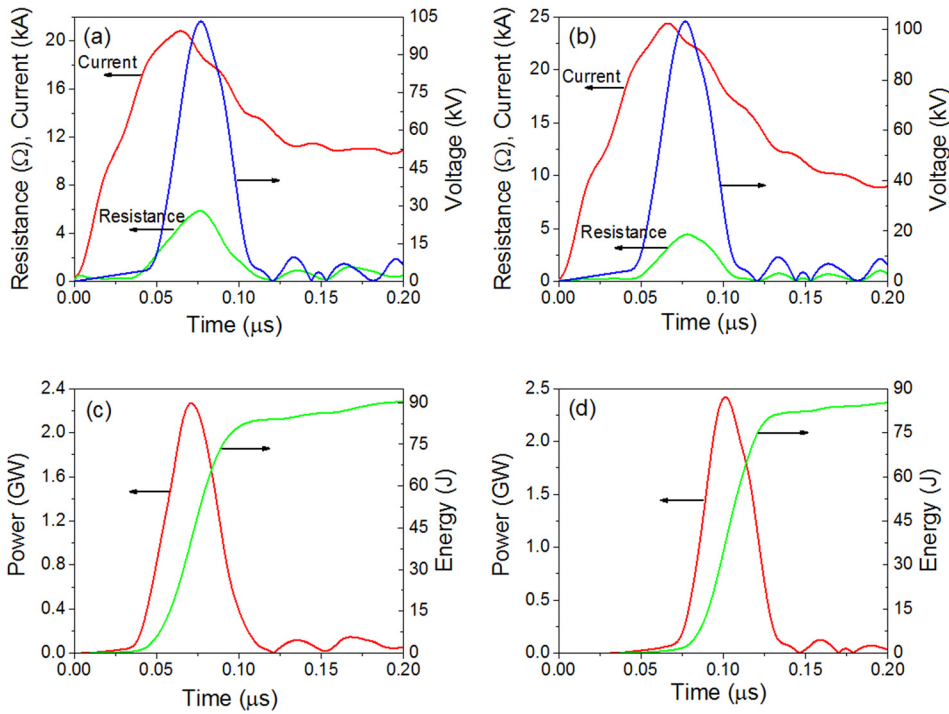


FIG. 2. Waveforms of the discharge current, resistive voltage, and wire resistance in the case of (a) Cu wire and (b) Al wire ns-timescale explosions in water. Power and energy temporal evolution for (c) Cu wire and (d) Al wire explosions.

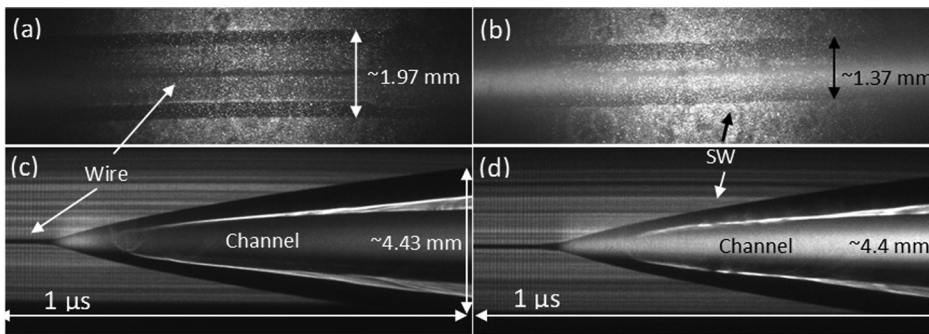


FIG. 3. Shadow framing images of the exploding (a) Cu and (b) Al wires in water. A frame duration of 3 ns and time delays of 290 ns for Cu and 190 ns for Al with respect to the beginning of the discharge current were used. Streak shadow images of the expanding exploded (c) Cu and (d) Al wires and the generated SWs.

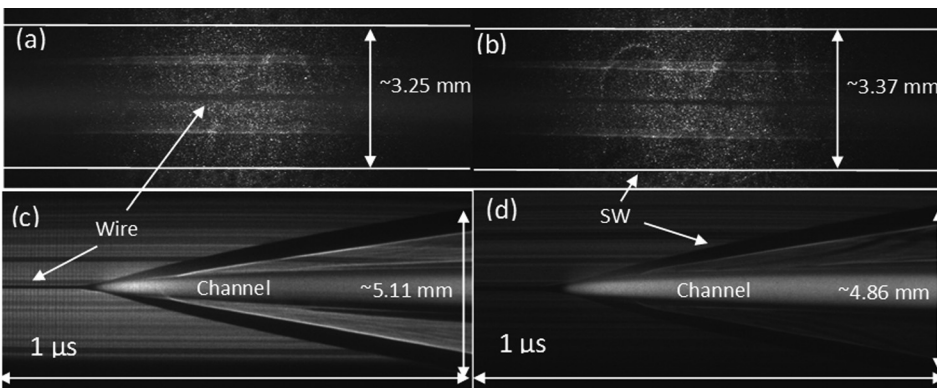


FIG. 4. Shadow framing image of the exploding (a) Cu and (b) Al wires in glycerol. A frame duration of 3 ns and time delays of 525 ns for Cu and 475 ns for Al with respect to the beginning of the discharge current were used. Streak shadow image of the expanding exploded (c) Cu and (d) Al wires and the generated SWs. The horizontal white lines in (a) and (b) represent the SWs because of insufficient visibility.

by the larger density of glycerol ( $1.26 \text{ g/cm}^3$ ) as compared to water ( $1 \text{ g/cm}^3$ ). Regarding the radial expansion velocity of the exploding Cu wire, one can see that at  $t \leq 13 \mu\text{s}$ , there is no detectable difference in these velocities obtained in water and glycerol. However, at  $t > 13 \mu\text{s}$ , faster radial expansion of the Cu wire for the case of its explosion in glycerol is obtained. Also, one can see that there are fast and slow phases in the SW propagation and exploded wire expansion. The radial expansion velocities of the SW and exploded Cu and Al wires in water and glycerol for the fast phase (at

$t \leq 300 \text{ ns}$ ) and the slow phase (at  $t \geq 1.5 \mu\text{s}$ ) are presented in Table I. One can see that although the SW propagates faster in glycerol, the wire expansion is faster in water. This can be explained by the lower density of water less resisting the wire's expansion.

Also, analysis of these radial trajectories shows that at  $t \sim 150 \text{ ns}$  with respect to the beginning of the discharge current, one obtains the fastest (up to  $\sim 4 \times 10^5 \text{ cm/s}$ ) radial expansion velocities of the wire and generated SW. Later, the SW expansion velocity decreases approaching the sound

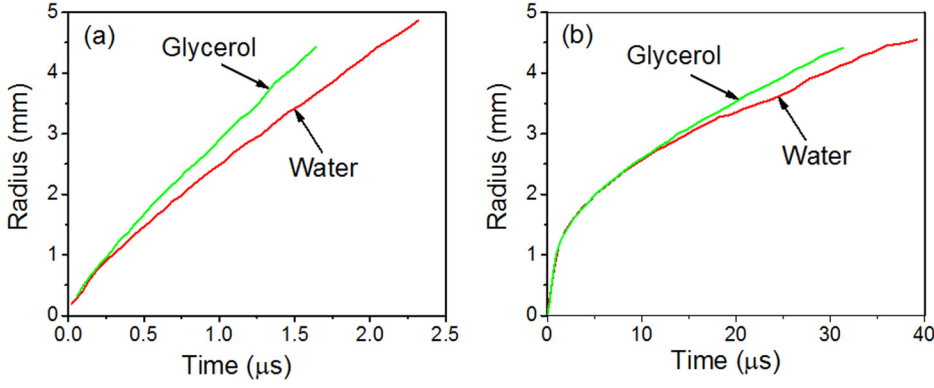


FIG. 5. Typical radial trajectories of the generated SW (a) and expanding Cu wire (b) versus time in water and glycerol.

TABLE I. Radial expansion velocities of the SW and exploded Cu wires (similar for Al wires' explosion) in water and glycerol for the fast phase (at  $t \approx 300$  ns) and the slow phase (at  $t \approx 1.5$   $\mu$ s).

		SW (water)	SW (glycerol)	Discharge channel (water)	Discharge channel (glycerol)
Fast phase	Velocity (m/s)	2370	2879	1330	1181
	Radius (mm)	0.95	1.07	0.52	0.43
Slow phase	Velocity (m/s)	1821	2141	269	263
	Radius (mm)	3.47	4.08	1.33	1.17

velocity at a radius  $r \geq 4$  mm. The wire's radial expansion velocity also decreases, and at  $t > 10$   $\mu$ s, it becomes almost constant and equal to  $\sim 50$  m/s.

A comparison between the SW radial trajectories obtained in the experiments and by 1D hydrodynamic simulations<sup>6</sup> of a Cu wire's underwater electrical explosion coupled with EOS of copper, aluminum, and water is shown in Fig. 6. One can see a satisfactory agreement between the experimental and simulation results. Also, using EOS of water and conservation of mass and momentum, one can evaluate the pressure using the measured velocity  $D$  of the SW<sup>13,14</sup>

$$D^2 = 3 \times 10^8 \left[ \left( \frac{\rho}{\rho_0} \right)^{7.15} - 1 \right] / [\rho_0(1 - \rho_0/\rho)],$$

$$P - P_0 = 3 \times 10^8 \left[ \left( \frac{\rho}{\rho_0} \right)^{7.15} - 1 \right], \quad (1)$$

where  $\rho$  and  $P$  are the density and pressure behind the SW front, respectively, and the subscript "0" indicates the normal conditions of water behind the SW front. The comparison between the calculated and simulated pressures is shown in Fig. 6(b), and again, one can see satisfactory agreement.

In the case of wire explosions in glycerol, 1D HD simulations were not applied because of the absence of available EOS for this liquid. Therefore, the pressure behind the SW front was calculated using a semi-empirical equation<sup>15</sup>

$$P_1 = P_0 + \rho_0 D(D - c)/S, \quad (2)$$

where  $c$  is the sound velocity in glycerol and  $S$  is a constant obtained experimentally in the range of 1.59–2.2. The comparison of the pressures behind the SW front in the cases of Cu wires' electrical explosions in water and glycerol (see Fig. 7) showed that within the first  $\sim 2$  mm of the SW's propagation, the pressure is significantly higher for the case of a wire explosion in glycerol.

To summarize the analysis of the shadow and streak images, one can state that electrical explosion of Al and Cu wires in glycerol results in faster propagation of the generated SW, larger pressure behind the SW front, and larger density of the exploded wires due to slower radial expansion. Thus, these data indicate the possible combustion of glycerol, leading to additional energy deposition (1 g of glycerol combustion results in 16 kJ of chemical energy) in the water flow.

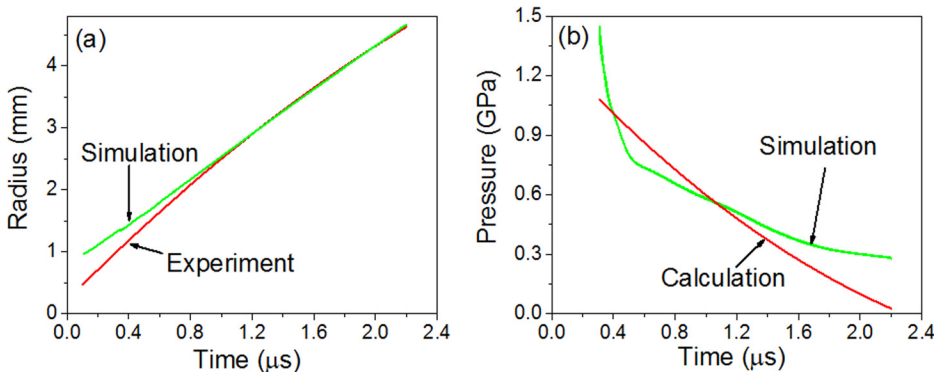


FIG. 6. (a) Measured and simulated position of the SW in water. (b) Calculated and simulated pressure behind the SW front.

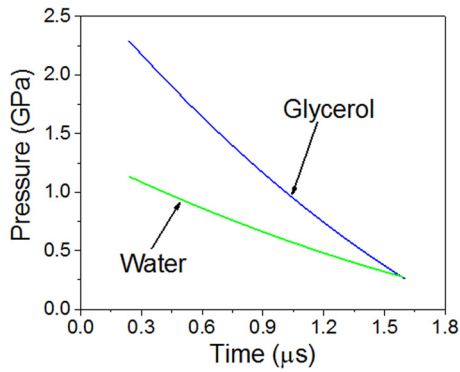


FIG. 7. Pressure calculations behind the front of the SW generated by a Cu wire electrical explosion in water and glycerol.

Although there was no noticeable difference between the expansion velocities of the discharge channel for the cases of Al and Cu wires' explosion in the same medium, there was a significant difference in the intensity of the light emitted by the exploding wires. Typical streak images of the self-light emission from the exploding Cu and Al wires in water and their intensity integrated along the vertical (radius) axis versus time are shown in Fig. 8. One can see a bright light emission during the first  $\sim 50$  ns from the beginning of the explosion (i.e., from the beginning of the fast decrease in the discharge current) when the main energy deposition into the wire is realized. These intensities are almost equal to each other for the cases of Al and Cu wire explosions. However, later in time ( $>100$  ns), one obtains the decrease in the light emission for the case of the Cu wire explosion and a gradual increase in the light emission for the case of the Al wire explosion. The decrease in the light emission intensity in the case of the Cu wire was also observed in earlier studies,<sup>4</sup> and it was explained by the decrease in the wire's surface temperature. Further in time ( $>200$  ns), for the case of Cu wire explosion, one obtains a gradual increase in the light emission intensity, which was explained by the increase in the flux of photons emitted by the inner layers of the Cu wire during its radial expansion.<sup>4</sup>

The ratio between the relative light emission intensities obtained in the case of Al and Cu wires' electrical explosions in water and the calculated temperatures of the surface of the wires versus time is shown in Fig. 9(a). One can see that the maximal ratio of light emission intensity between Al and Cu is  $\sim 1.7$ . The surface temperature of the exploding wires was obtained using the results of 1D HD simulations<sup>6</sup> coupled

with EOS for Cu, Al, and water. In these simulations, the experimentally obtained energy deposition into the wires was used as an input for the simulation. Here, let us note that these simulations did not take into account the possible combustion of Al. One can see in Fig. 9(b) that the temporal behavior of the surface temperature is almost the same and even the temperature of the Cu wire's surface is slightly larger than the temperature of the Al wire's surface. The latter can be explained by a larger energy density deposition in the case of a Cu wire explosion ( $\sim 17$  eV) than in the case of an Al wire explosion ( $\sim 14$  eV). These data contradict the streak images of the self-emission of exploding Cu and Al wires in water and glycerol (see Fig. 8) and the laser backlit images obtained at a  $50 \mu\text{s}$  time-scale (see Fig. 10). These streak images showed brighter and longer duration of the light emission in the case of Al wire explosion. Thus, one can consider that the possible source of more intense light radiation is Al combustion. Also, one can see that the duration of the light emission for both Cu and Al wire explosions is significantly longer in glycerol than in water, which is probably related to glycerol combustion.

The maximal energy  $\Delta E$  which can be realized as a result of combustion<sup>18</sup> of the Al wire having a weight of 1.54 mg,  $4Al + 3O_2 \rightarrow 2Al_2O_3 + \Delta H(32.75 \text{ kJ/g})$ , is  $\Delta E \sim 31.24 J$ . This energy is more than twice smaller than the electrical energy deposited into the Al wire (see Fig. 2). Next, we artificially increased the energy deposited into the Al wire in the 1D HD simulation, in order to obtain the Al wire surface temperature (assuming black-body radiation) which satisfies the experimentally obtained ratio between Al and Cu wires' light intensities,  $\max(T_{Al}^4/T_{Cu}^4) \sim 1.7$ . The results of these simulations showed that one has to add  $\sim 15 J$ , in order to satisfy this experimentally obtained ratio. This,  $\sim 15 J$ , additional energy which corresponds to  $\sim 0.48$  mg can be related to  $\sim 30\%$  of Al wire material combustion.

## B. Microsecond timescale underwater electrical explosion of Cu and Al wires

The experiments on electrical explosions of Cu and Al wires in water and glycerol were repeated on the  $\mu\text{s}$ -time-scale in order to check whether the effect of Al and glycerol combustion is stronger in these time durations. In these experiments, 4.5 cm length Al and Cu wires with diameters of  $250 \mu\text{m}$  and  $200 \mu\text{m}$ , respectively, were used. Typical waveforms of the discharge current and resistive voltage for the case of Cu and Al wires' electrical explosion in water are

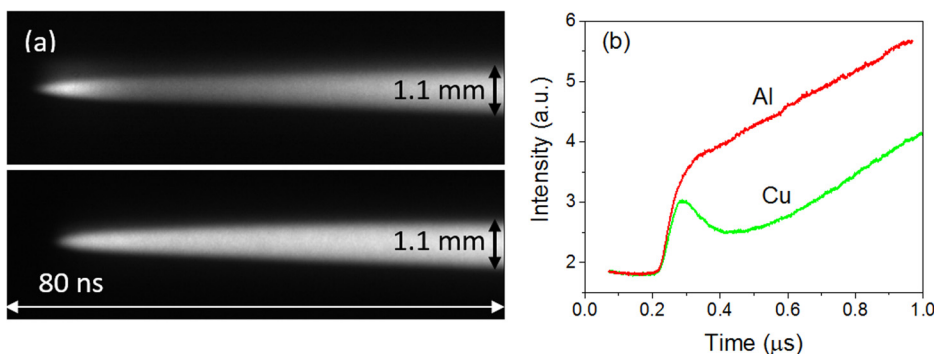


FIG. 8. Typical streak images of the self-light emission from the exploding Cu (a) and Al (b) wires in water and their intensity integrated along the vertical axis versus time. These streak ( $50 \text{ ns/mm}$ ) images were obtained with a low pass optical filter of  $700 \text{ nm}$ .

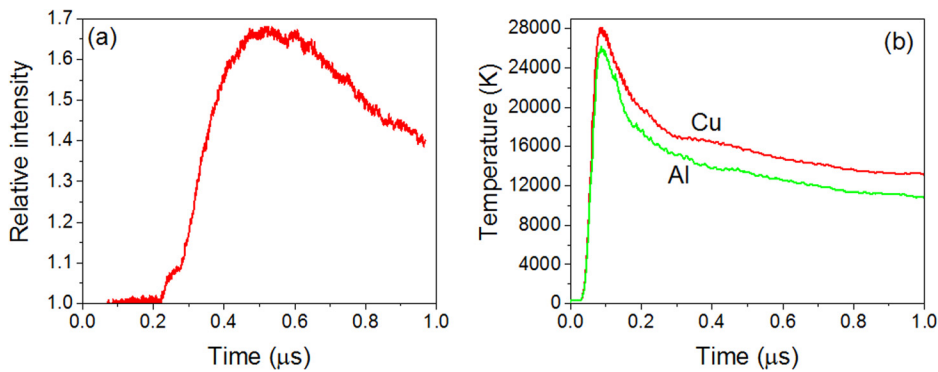


FIG. 9. (a) Ratio between relative light emission intensities obtained in the case of Al and Cu wires' electrical explosions in water; (b) simulated temperature at the surface of the Al and Cu wires during the explosion.

shown in Figs. 11(a) and 11(b), together with temporal evolution of the wires' resistance. The time dependent power and energy deposited into Cu and Al wires are shown in Figs. 11(c) and 11(d). Similar waveforms of the current and voltage were obtained in the case of Cu and Al wire electrical explosions in glycerol. One can see that the waveforms of the current and resistive voltage are almost the same except that in the case of the Al wire explosion, the discharge current drops to almost zero. The latter results in the gradual increase in the resistance of the discharge channel. In the case of Cu wire explosions, one obtains a current of  $\sim 1$  kA continuing to flow through the discharge channel. These data indicate that Al wire explosion is characterized by the formation of a discharge channel with smaller conductivity. Average current densities, calculated at the maximum of the discharge current and accounting the radial expansion of wires (see Fig. 12), were  $\sim 5.5 \times 10^6$  A/cm<sup>2</sup> and  $\sim 7.5 \times 10^6$  A/cm<sup>2</sup> for Cu and Al wires' explosions, respectively. Also, the energy density deposition in these explosions was 24 kJ/g (16 eV/atom) and 50 kJ/g (14 eV/atom) for Cu and Al wires' explosions, respectively. Here, let us note that one requires  $\sim 76$  J and  $\sim 61$  J for complete

vaporization of the Cu and Al wires, respectively, which are significantly smaller than the  $\sim 300$  J deposited energy.

Shadow streak ( $250$  ns/mm) images of Cu and Al wires'  $\mu$ s-timescale explosions in water and glycerol are shown in Fig. 12. One can see weak SWs generated prior to the wire explosion. These weak SWs are associated with the phase transitions which the wire experiences during the rise time of the discharge current.<sup>17</sup> Similar to the case of the ns-timescale explosions, no detectable difference was obtained in the velocities of the generated SWs and plasma channels for Cu and Al wire explosions in the same medium. However, similar to the ns-timescale, there is an increase in the SW's velocity when comparing water with glycerol wires' explosions (see Table II). Moreover, in the case of  $\mu$ s-timescale explosions, this increase is almost 15% larger than in the case of ns-timescale wires' explosions. Also, while on the ns-timescale, the plasma channel radial expansion was slower in the case of explosion in glycerol, in  $\mu$ s-timescale explosions, one obtains an opposite result. Namely, radial expansion of the plasma channel is significantly faster in the case of wire electrical explosion in glycerol. These data indicate glycerol combustion becoming more noticeable in  $\mu$ s-timescale explosions.

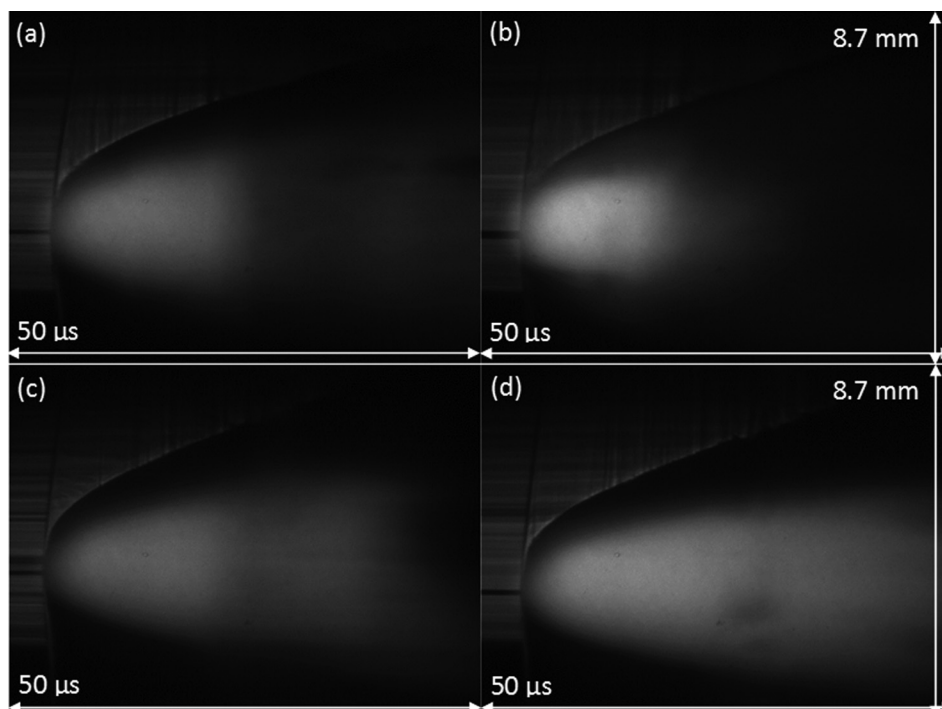


FIG. 10. Typical laser backlit streak images ( $2.5 \mu$ s/mm) of exploding Cu (a) and Al (b) wires in water and Cu (c) and Al (d) wires in glycerol.

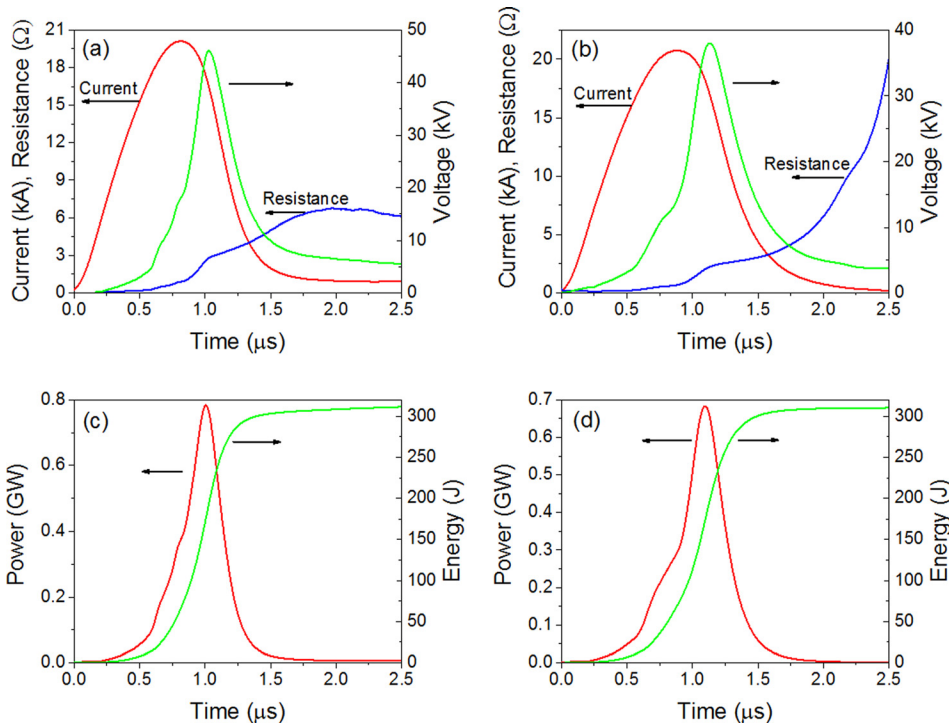


FIG. 11. Waveforms of discharge current, resistive voltage, and wire resistance in the case of (a) Cu wire and (b) Al wire electrical underwater explosions. Power and energy temporal evolution for (c) Cu and (d) Al wire explosions.

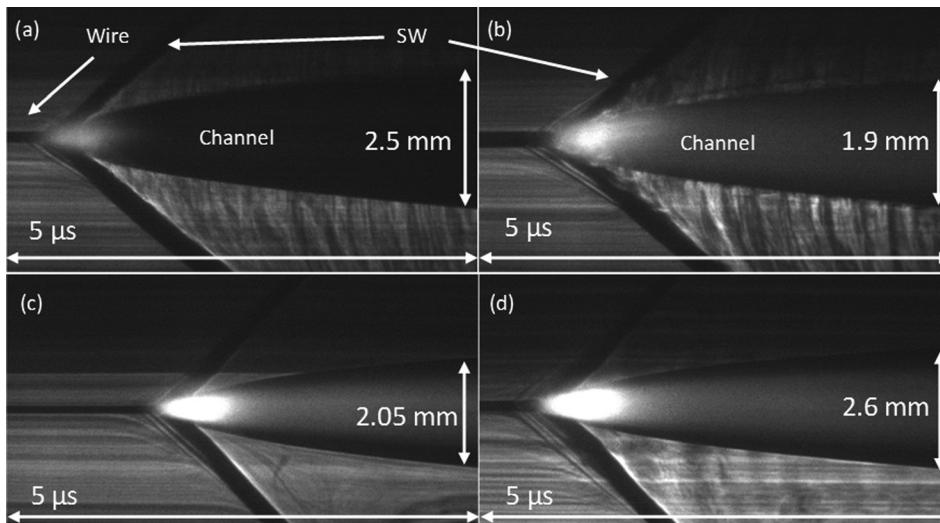


FIG. 12. Typical laser backlit streak images with a streak of 250 ns/mm. Explosion of (a) Cu and (b) Al wires in water and (c) Cu and (d) Al wires in glycerol.

TABLE II. Radial velocities of the SW and exploded Cu wires (similar to Al wires' explosion) in water and glycerol for the fast phase (at  $t \approx 800$  ns) and the slow phase (at  $t \approx 2 \mu\text{s}$ ).

		SW (water)	SW (glycerol)	Discharge channel (water)	Discharge channel (glycerol)
Fast phase	Velocity (m/s)	1575	2211	513	613
	Radius (mm)	0.89	0.91	0.37	0.33
Slow phase	Velocity (m/s)	1501	2200	79	274
	Radius (mm)	2.74	3.56	0.72	0.86

Laser backlit streak images showed that the intensity of the light emission from the exploded Al wire is higher than that from the exploded Cu wire, in both water and glycerol. Moreover, in the case of the longer ( $2.5 \mu\text{s}/\text{mm}$ ) streak shadow images (see Fig. 13), the light emission from the Al plasma channel is clearly stronger in water than light emission from the Cu plasma channel. However, in the case of explosion in

glycerol, light emission intensities from Cu and Al plasma channels are roughly the same. The latter can be related to decreased transparency of glycerol at long timescales as well as to the low sensitivity of the camera. Nevertheless, the obtained streak images strongly indicate Al combustion.

Next, we present in Fig. 14 the results of 1D HD simulations for the  $\mu\text{s}$ -timescale explosion of a Cu wire in water

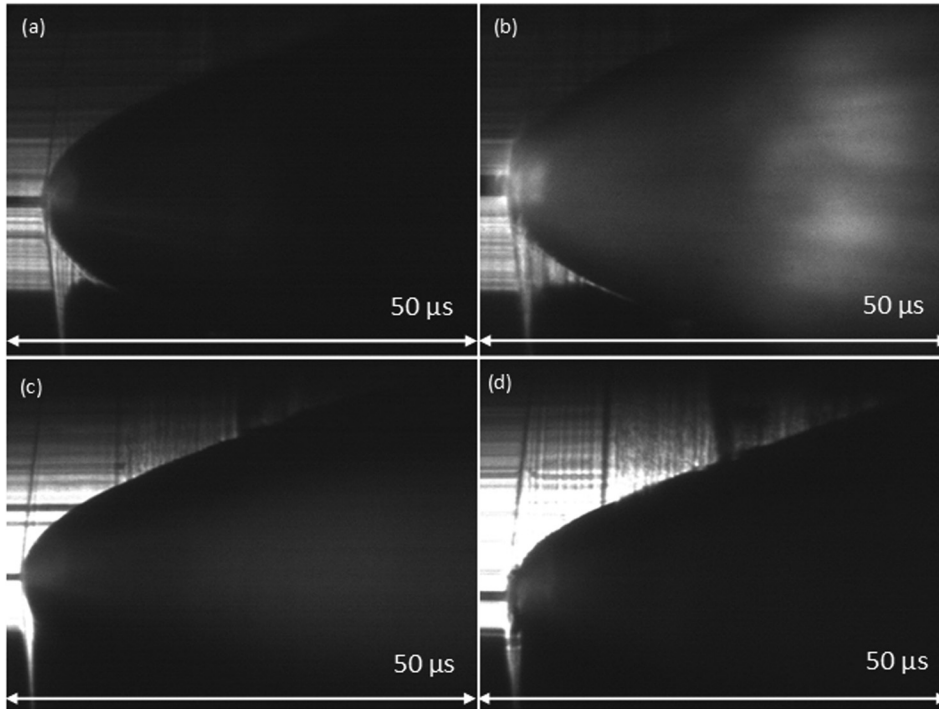


FIG. 13. Typical laser backlit streak images with a streak of  $2.5 \mu\text{s}/\text{mm}$ . Explosion of (a) Cu and (b) Al wires in water and (c) Cu and (d) Al wires in glycerol.

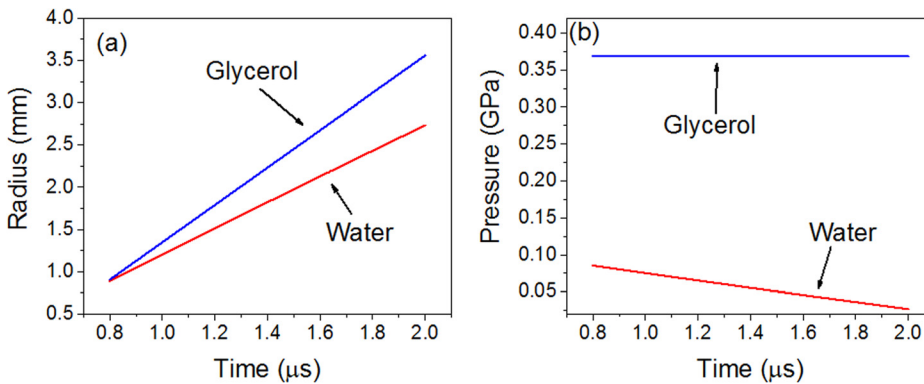


FIG. 14. Plot of the (a) radius of the SWs as a function of time with respect to the beginning of the discharge current and (b) calculated pressure behind the SW front for water and glycerol. Here,  $t \sim 750 \text{ ns}$  is the time of the wire electrical explosion.

and glycerol, namely, the temporal evolution of the SW radius and pressure behind the SW front. Similar to ns-timescale explosions, the pressure behind the SW generated during  $\mu\text{s}$ -timescale explosion in glycerol is significantly larger than that in the case of wire explosions in water and the value of this pressure is almost constant. The latter results from an almost straight line of the SW trajectory shown in Fig. 12. These data strongly indicate glycerol combustion whose energy keeps a high pressure behind the front of the SW despite its radial expansion. Also, one can see that the highest value of the pressure is smaller than that in the case of the ns-timescale Cu wire explosions ( $>4 \text{ GPa}$ ). The latter can be explained by a significantly lower power deposition rate<sup>4</sup> in  $\mu\text{s}$ -timescale explosion of  $\sim 1.6 \times 10^{15} \text{ W/s}$  than that in ns-timescale experiments of  $\sim 4.4 \times 10^{16} \text{ W/s}$ .

#### IV. DISCUSSION

In earlier research,<sup>19</sup> it was shown that despite a very high temperature of the wire's surface reaching  $\sim 1 \text{ eV}$ , the adjacent water layer may remain in a liquid phase because of

high pressure. However, due to a radiation flux emitted by the exploding wire,<sup>16</sup> one obtains ionization of a thin ( $\leq 1 \mu\text{m}$ ) layer of water in the vicinity of the exploding wire's surface. At the beginning of explosion, the combustion of Al can be obtained only at the surface of the wire, which is in contact with the ionized thin layer of water. Later in time, due to a diffusion process of the Al atoms and ions, internal layers of the Al plasma come into contact with ionized water.

Let us consider a nanosecond electrical explosion of an Al wire in water. The radius of the Al wire is  $r_0 = 63.5 \mu\text{m} = 6.35 \times 10^{-3} \text{ cm}$ . The length of the Al wire is  $l_0 = 4.5 \text{ cm}$ , its initial volume is  $Q = \pi l_0 r_0^2 \approx 5.6 \times 10^{-4} \text{ cm}^3$ , the total mass is  $M \approx 1.54 \text{ mg}$ , and the total number of Al atoms in this wire is  $N \approx 3.4 \times 10^{19}$ . The density of Al atoms at normal conditions is  $\rho N_a / M = 6 \times 10^{22} \text{ cm}^{-3}$ , where  $N_a$  is the Avogadro number and  $M$  is the molar weight of Al. After the wire explosion, behind the front of the cylindrical SW, one obtains a cylindrical volume filled with the Al plasma, which expands radially, and during a time  $\tau \approx 1 \mu\text{s}$ , the radius of this plasma reaches  $R(\tau) \approx 7 \times 10^{-2} \text{ cm}$ . This allows one to

make an estimate of an average radial plasma velocity as  $\bar{v}_p \approx 7 \times 10^4$  cm/s. Assuming a uniform radial distribution of the plasma density, one can estimate its time-dependent value as  $\rho(t) \approx \rho_0[r_0/R(t)]^2$  and at  $R(t) > 0.01$  cm, the density of the Al plasma becomes smaller than the density of water (the normal density of water is  $n \approx 3.3 \times 10^{22}$  cm $^{-3}$ ) located between the plasma and the SW front. Here, let us note that the water density remains almost constant. The density flux of water molecule diffusion through the boundary of the plasma can be calculated as

$$J = D\partial n/\partial r. \quad (3)$$

Here,  $D$  is the diffusion coefficient which can be estimated as<sup>20</sup>

$$D = kT/\pi m_* n d_{12}^2 \sqrt{v_1^2 + v_2^2}, \quad (4)$$

where  $m_* = m_{\text{Al}}m_{\text{H}_2\text{O}}/(m_{\text{Al}} + m_{\text{H}_2\text{O}}) \approx 18 \times 10^{-24}$  g is the reduced mass of Al atoms and water molecules,  $d_{12} = (d_1 + d_2)/2 \approx 1.84 \times 10^{-8}$  cm is the average diameter of an Al atom and a water molecule, and  $v_1$  and  $v_2$  are the thermal velocities of the Al atoms and water molecules, respectively, having the same temperature. Considering two values of temperature, namely  $T_1 = 10^3$  K and  $T_2 = 10^4$  K, one obtains diffusion coefficients of  $D_1 \approx 5.4 \times 10^{-3}$  cm $^2$ /s and  $D_2 = 5.4 \times 10^{-2}$  cm $^2$ /s. The typical mean free path length of a water molecule can be estimated as  $\lambda \approx (nd_{12})^{-1} \approx 10^{-7}$  cm. Thus, the “diffusion velocity,” defined as  $D/\lambda$ , will be either  $5.4 \times 10^4$  cm/s (1000 °K) or  $5.4 \times 10^5$  cm/s (10000 °K). These velocities are comparable to or larger than the average velocity of the Al wire expansion. Therefore, one can consider that during the Al wire expansion, water molecules can penetrate the expanding boundary layer of the Al plasma and the combustion of this boundary layer can be obtained. Due to the fast radial expansion of the plasma channel accompanied by water molecule diffusion, new layers of Al atoms can be involved in the combustion process. In the case of the total combustion of the Al wire, the maximal energy realized will be  $\sim 31$  J, but an average rate of the energy realized is only  $\leq 5 \times 10^7$  J/s which is  $\sim 10$  times smaller than the rate of the energy deposited into the water flow by the wire expansion,  $\sim 4 \cdot 10^8$  J/s. This estimate gives the maximal value of the energy rate of the additional energy deposited into the water flow. Indeed, during the first few hundreds of ns with respect to the wire explosion, when expanding wire can be considered as a “piston” for generated SW, the combustion of Al occurs from the Al plasma cylinder having a smaller diameter, and a smaller number of Al atoms are involved in the combustion process. This explains why the combustion of Al did not contribute to the velocities of the SWs generated by Al wire explosion.

At normal pressure, glycerol auto-ignition<sup>20</sup> begins at the temperature  $T > 370$  °K and this combustion becomes efficient at  $T \geq 1000$  °K, resulting in a chemical energy of 16 kJ/g. The increase in temperature and pressure leads to the decrease in time of the glycerol ignition. In the present experimental conditions, when the temperature at the surface of the exploding wires exceeds  $> 1000$  °K and the pressure is

in the range of  $10^9$ – $10^8$  Pa, one can expect efficient combustion of glycerol in the vicinity of the exploding wire. It is understood that the process of the glycerol combustion at such extreme conditions requires additional research. Nevertheless, the experimental data indicate that this combustion process contributes significantly to the velocity of the generated SW and larger pressure build-up behind the SW front.

## V. SUMMARY

The experimental research carried out on single Cu and Al wire electrical explosions in water and glycerol on ns- and  $\mu$ s-timescales showed evidence of Al combustion. However, this combustion does not contribute to the velocity of the generated SW because of a relatively slow rate of energy density deposition into the water flow. Also, it was shown that in the case of Cu and Al wire electrical explosion in glycerol, higher density of glycerol and its combustion result in higher SW velocity and consequently higher pressure behind the SW front.

## ACKNOWLEDGMENTS

We are grateful to V. Gurovich for fruitful discussions and S. Gleizer for assistance in experiments.

- <sup>1</sup>V. E. Fortov and I. T. Iakubov, *The Physics of Non-Ideal Plasma* (World Scientific, Singapore, 2000).
- <sup>2</sup>W. DeSilva and J. D. Katsouras, *Phys. Rev. E* **57**, 5945 (1998).
- <sup>3</sup>Ya. E. Krasik, S. Efimov, D. Sheftman, A. Fedotov-Gefen, O. Antonov, D. Shafer, D. Yanuka, M. Nitishinskiy, M. Kozlov, L. Gilburd, G. Toker, S. Gleizer, E. Zvulun, V. Tz. Gurovich, D. Varentsov, and M. Rodionova, *IEEE Trans. Plasma Sci.* **44**, 412 (2016).
- <sup>4</sup>A. Grinenko, Ya. E. Krasik, S. Efimov, A. Fedotov, and V. Tz. Gurovich, *Phys. Plasmas* **13**, 042701 (2006).
- <sup>5</sup>L. Gilburd, S. Efimov, A. Fedotov Gefen, V. Tz. Gurovich, G. Bazalitzki, O. Antonov, and Ya. E. Krasik, *Laser Part. Beams* **30**, 215 (2012).
- <sup>6</sup>O. Antonov, L. Gilburd, S. Efimov, G. Bazalitzki, V. Tz. Gurovich, and Ya. E. Krasik, *Phys. Plasmas* **19**, 102702 (2012).
- <sup>7</sup>S. Efimov, L. Gilburd, A. Fedotov-Gefen, V. Tz. Gurovich, J. Felsteiner, and Ya. E. Krasik, *Shock Waves* **22**, 207 (2012).
- <sup>8</sup>V. S. Sedoi, G. A. Mesyats, V. I. Oreshkin, V. V. Valevich, and L. I. Chemezova, *IEEE Trans. Plasma Sci.* **27**, 845 (1999).
- <sup>9</sup>Yu. A. Kotov, O. M. Samatov, V. S. Sedoi, L. I. Chemezova, and A. A. Chertov, *MegaGauss Fields and Pulsed Power Systems*, edited by V. Titov and G. Shvetsov (Nova Science, New York, 1990), pp. 497–502.
- <sup>10</sup>V. I. Oreshkin, S. A. Barenhol'ts, and S. A. Chaikovskiy, *Tech. Phys.* **52**, 642 (2007).
- <sup>11</sup>S. A. Chaikovskiy, V. I. Oreshkin, I. M. Datsko, N. A. Labetskaya, D. V. Rybka, and N. A. Ratakhin, *Phys. Plasmas* **22**, 112704 (2015).
- <sup>12</sup>V. I. Oreshkin, *Phys. Plasmas* **15**, 092103 (2008).
- <sup>13</sup>G. B. Whitham, *Linear and Nonlinear Waves* (Wiley, New York, 1974).
- <sup>14</sup>Y. B. Zeldovich and Y. P. Raizer, *Physics of Shock Waves and High-Temperature Hydrodynamic Phenomena*, 2nd ed. (Academic, New York, 1967).
- <sup>15</sup>S. V. Uvarov, I. A. Bannikova, and O. B. Naimark, “Pulse loading of glycerol by electric explosion of wire,” *J. Phys.: Conf. Ser.* **653**, 012034 (2015).
- <sup>16</sup>A. F. Belyayev, Yu. V. Frolov, and A. I. Korotkov, *Fiz. Gor. Vzryva* **4**, 323 (1968).
- <sup>17</sup>A. Fedotov, D. Sheftman, V. Tz. Gurovich, S. Efimov, G. Bazalitzki, Ya. E. Krasik, and V. I. Oreshkin, *Phys. Plasmas* **15**, 082704 (2008).
- <sup>18</sup>A. Grinenko, A. Sayapin, V. Tz. Gurovich, S. Efimov, J. Felsteiner, and Ya. E. Krasik, *J. Appl. Phys.* **97**, 023303 (2005).
- <sup>19</sup>A. Grinenko, V. Tz. Gurovich, Ya. E. Krasik, and Yu. Dolinsky, *J. Appl. Phys.* **100**, 113309 (2006).
- <sup>20</sup>K. Grab-Rogalinski and S. Szwaja, *IOP Conf. Ser.: Mater. Sci. Eng.* **148**, 012066 (2016).